Brackish springs in coastal aquifers and the role of calcite dissolution by mixing waters

Esteban Sanz Escudé

October 19, 2007

CHAPTER 6: POROSITY DEVELOPMENT IN CARBONATE COASTAL AQUIFERS BY MIXING WATERS

PhD Thesis
Department of Geotechnical Engineering and Geo-Sciences (ETCG)
Technical University of Catalonia (UPC)

Supervisors:
Dr. Jesús Carrera Ramírez
Dr. Carlos Ayora Ibáñez

Institute of Earth Sciences 'Jaume Almera', CSIC

Chapter 6

Porosity development in carbonate coastal aquifers by mixing waters

Coastal carbonate aquifers often represent a source of high quality water, which can be contaminated by seawater intrusion phenomena. Therefore, these aquifers have received a special attention not only because of seawater intrusion caused by heavy pumping (Tulipano, 2003), but also because of the complex and interesting geochemical processes associated with the saltwater mixing zone. These lead to a wide variety of features such as large-scale dissolution causing cave formation, fabric-selective associated aragonite dissolution and calcite precipitation, and dolomitization (Runnels, 1969; Plummer, 1975; Hanshaw and Back, 1979; Tucker and Wright, 1990; Raeisi and Mylroie, 1995).

The theory is based on the fact that when two solutions are mixed, concentrations in the mixture are volume-weighted averages of the two end-members, but the thermodynamic activities of the species controlling the water-mineral reactions are non-linear functions of the mixing ratio. Therefore, two end-member solutions in equilibrium with a solid phase could lead to a mixture either under or supersaturated. Wigley and Plummer (1976) listed the most important factors controlling the saturation of carbonate minerals in water mixtures, including the differences in ionic strength, pCO_2, temperature, or ion activity of Ca^{2+} and CO_3^{2-} in the two end members. The fact

that both over and under saturation may occur is due mainly to the interplay of ionic strength and algebraic effects, which oppose each other. An increase in ionic strength causes a reduction in ion activity (i.e. an increase in solubility). This reduction is much more marked for low than for high salinities. As a result, a mixture of two waters saturated in calcite but with different salinities would tend to be undersaturated, especially for low mixing ratios (more fresh than salt water in the mixture). On the other hand, it is easy to show that, when two waters saturated with respect to a mineral mix, the mixture would be oversaturated if variations in activity coefficients are neglected. This is termed algebraic effect. These two effects are superimposed to others, such as changes in speciation. As a result, it is not trivial to anticipate whether over or undersaturation will result from a mixture.

Calcite undersaturation and/or carbonate dissolution has been reported in several mixing zones around the world. Thus, the coastal mixing zone of the Yucatan Peninsula is undersaturated with respect to calcite and aragonite over a wide range of salinities, and the dissolution of these minerals is considered a major geomorphic process in developing caves, coves and crescent-shaped beaches along the Yucatan coast (Back et al. 1979; Hanshaw and Back, 1980; Back et al. 1986; Stossell et al. 1989). Ng and Jones (1995) studied the geochemistry of Grand Cayman and found that simple mixing of fresh and seawater could not explain water chemistry of the boreholes, but different processes including dissolution and precipitation of calcite and dolomite have to be considered. Smart et al. (1988) and Whitaker and Smart (1997) reported the results of chemical and rock profiling through the modern mixing zone on Andros Island in the Bahamas. They show calcite undersaturation close to the seawater end of the mixing zone intercepted in submarine cavities. These authors postulated that oxidation of organic matter produces additional CO_2 and significantly enhances this undersaturation.

On the other hand, some mixing zones are also reported where calcite undersaturation does not take place. Plummer et al. (1976) concluded that mixing of fresh and seawater is not significant in controlling calcite saturation in the Bermudas coast. Most of the groundwater samples from a dune aquifer near Coos Bay, Oregon, and from a coastal carbonate aquifer in Mallorca, were saturated with respect to calcite and dolomite (Magaritz and Luzier, 1985; Price and Herman, 1991). Wicks et al. (1995) and Wicks and Herman (1996) documented that gypsum dissolution generates a solution capable of precipitating calcite in the mixing zone of upper Floridian aquifer. Maliva et al. (2001) documented that no change in mineralogy, cement type or porosity can be correlated with current or recent location of a mixing zone in the Biscayne aquifer, Florida. Melim et al. (2002) used evidence from the Neogene from Bahamas to conclude that mixing zone diagenesis includes aragonite dissolution and minor low-magnesium calcite cementation but does not show the cavernous porosity predicted by the diagenetic models for the mixing zone.

The above studies reflect that the dissolution potential of carbonates in the mixing zone can be diverse, ranging from cases with no apparent dissolution (Bermudas, Florida) to cases with high dissolution rate (Yucatan, Bahamas). It is interesting to note that the dissolution/precipitation features display some relationship with the water/rock ratio. Thus, undersaturation is described for high ratios (e.g. open cave voids) where mixing is enhanced. In contrast, no explicit dissolution or supersaturation is described for low ratios (e.g. boreholes). The dissolution features described could be alternatively attributed to variations in the chemistry of the two end members, which may alter significantly the dissolution potential of the mixture. When evaluating dissolution rates, however, the rate at which the two end-members mix has an important effect on the dissolution potential of the mixture. In fact, this prompted Sanford and Konikow (1989) to couple dissolution with transport. They used a two-step method consisting basically of (1) transporting TDS and dissolved calcite, (2) evaluating at each node the dissolution potential (derived from the mixing ratio), and (3) dissolving the deficit. They predicted that appreciable carbonate dissolution might occur due to mixing of fresh and seawater. Their results were based on the dimension scale and discharge rates associated with the Yucatan continental platform, obtaining significantly less potential dissolution for a small island. Sanford and Konikow (1989) model has influenced later work on seawater intrusion in carbonate areas (e.g. Mylroie and Carew, 1990; Mylroie et al., 1991). However, this model might suffer from two limitations. First, the two-step method distributes dissolution during a time step. So, even if dissolution is assumed to take place in equilibrium, it is effectively simulated as kinetic, with a reaction rate inversely proportional to the adopted time increment. This might affect not only computed rates, but also the spatial distribution of dissolution. Second, only one aqueous component (dissolved calcite) is transported (many species are transported, but in proportions predefined by their speciation at equilibrium with calcite). We conjecture that changes in speciation during dissolution might enhance the transport of some species, thus changing the conditions under which dissolution potential was evaluated.

The objective of our work is precisely to test the above conjectures and analyse the effect that simplifications of the double step method have on dissolution potential in the saltwater mixing zone of coastal aquifers. To this end, we use fully coupled reactive transport modeling. First, we compare the latter with the two-step approach on a simple 1D diffusion problem. This sheds some light on the processes controlling dissolution rate, which allows us to revise the results of the 2D saline intrusion case analysed by Sanford and Konikow (1989).

6.1. Hydrogeochemistry

To represent the calcite-water system we selected 24 species: H^+, OH^-, Ca^{2+}, CO_3^{2-}, HCO_3^-, $CO_2(aq)$, $CaHCO_3^+$, $CaCO_3(aq)$, Mg^{2+}, $MgHCO_3^+$, $MgCO_3(aq)$, $MgOH^-$, K^+, Na^+, $NaHCO_3(aq)$,

$NaCO_3^-$, Cl^-, SO_4^{2-}, $CaSO_4$(aq), $MgSO_4$(aq), KSO_4^-, $NaSO_4^-$, CO_2(g) and $CaCO_3$(calcite). Chemical composition of the initial and boundary solutions used in the study are listed in Table 6.1. Solution #1 represents an open ocean water (Sanford and Konikow, 1989) which presents a relatively high pH and low P_{CO2}. However, once seawater enters a carbonate aquifer, the solution may be affected by changes in pressure and temperature, water-rock interaction processes, organic matter oxidation and re-oxidation of reduced sulphur (Whitaker and Smart, 1997). Because of these processes, saline ground water often displays higher P_{CO2}, lower pH and lower calcite saturation index than that of open ocean water. This is the case of solution #2, obtained from boreholes in a coastal aquifer from Grand Cayman (Ng and Jones, 1995). Solution #3 is a modification of solution #2 in which calcite was dissolved to equilibrium.

Different low salinity end-member solutions (solutions #4 and 5, in Table 6.1) were calculated by dissolving calcite to equilibrium in distilled water, in equilibrium with $P_{CO2}=10^{-2.0}$ or $10^{-3.0}$. These solutions are assumed to represent fresh groundwater in limestone regions, where the different values of P_{CO2} may be due to varying degrees of organic activity in the soil (Brook et al., 1983). In addition, different equilibrium points can be attained with different calcium concentrations: either higher (e.g. increased by gypsum dissolution), or lower (e.g. decreased by cation exchange or gypsum precipitation) (Kim et al., 2003). In such cases, if the P_{CO2} and calcite saturation of the solution remain constant, the solutions will present different pH values. We considered two additional calcite saturated solutions, a distilled water in equilibrium with gypsum (pH 6.97), and another with a low calcium concentration and pH 7.73 (solutions #6 and 7, Table 6.1). Both solutions are equilibrated with calcite at $P_{CO2}=10^{-2.0}$.

Table 6.1: Chemical composition of boundary solutions used in the calculations. Units for (total) concentrations are mmol kg_{water}^{-1}; units for Pressure are bar; Alk. is the alkalinity; SI_{Cc} is the Saturation Index of Calcite; I is the Ionic strength.

Solution #	pH	Ca	Mg	Na	K	Alk.	S	Cl	SI_{Cc}	Log P_{CO2}	I
(1) Open ocean water	8.22	10.66	55.10	485.00	10.60	2.41	29.30	566.00	0.76	-3.38	.675
(2) Saline groundwater	7.21	9.64	22.43	496.53	9.28	4.25	29.36	564.13	0.06	-2.01	.625
(3) Saline groundwat.-Cc	7.16	9.60	22.43	496.53	9.28	4.18	29.36	564.13	0.00	-1.96	.625
(4) Freshwater-(P_{CO2})	7.30	1.65	.0	.0	.0	3.29	.0	.0	.0	-2.00	.005
(5) Freshwater-(P_{CO2})	7.95	0.73	.0	.0	.0	1.46	.0	.0	.0	-3.00	.002
(6) Freshwater (P_{CO2}-Gy)	6.97	16.20	.0	.0	.0	1.81	15.30	.0	.0	-2.00	.043
(7) Freshwater-(P_{CO2}-pH)	7.73	0.24	.0	.0	.0	8.63	.0	.0	.0	-2.00	.005

Ref: (1) Sanford and Konikow (1989), (2) Ng and Jones (1995)

One must decide whether reactions are treated kinetically or in equilibrium, in order to couple hydrogeochistry and transport. Aqueous reactions are fast compared to transport rates and are usually considered in equilibrium. However, heterogeneous reactions, such as mineral dissolution or precipitation, may be slow or fast. In this work, we assumed equilibrium conditions for several reasons. First, from a conceptual viewpoint, calcite dissolution is fast relative to residence times in coastal aquifers, contrary to precipitation. This is consistent with field observations, which normally describe oversaturated or equilibrated waters (e.g. solutions 1 and 2 in Table 6.1), but not undersaturation (except at open spaces, such as caves, where residence times can be short). The situations described here refer to dissolution. Second, preliminary runs (not shown here) suggested the kinetic effects can be neglected when standard reaction rates (Inskeep and Bloom, 1985) are used.

6.2. Reactive transport modeling

The continuum representation of the multisolute reactive transport can be written as follows:

$$-q\nabla c_i + \nabla(\phi D \nabla c_i) + R_i(c_i) = \phi \frac{\partial c_i}{\partial t} \qquad (6.1)$$

where c_i is the concentration of the i-th species in solution (kmol m^{-3}), q is the darcian flux (m^3 m^{-2} s^{-1}), ϕ is the porosity, D is a term which includes the molecular diffusion and the mechanical dispersion (m^2s^{-1}), assumed equal for all species and R_i is a source/sink term of the solute due to the chemical reactions (kmol $m^{-3}s^{-1}$). Equation (6.1) is completed with appropriate initial and boundary conditions. These equations are coupled to chemical equations for representing either reaction rates (slow reactions) or equilibrium (fast reactions). We used the RETRASO code (Saaltink et al. 1998 and 2004), which solves simultaneously the aqueous complexation reactions, the dissolution /precipitation reactions and the transport terms. This method is called the 'direct substitution approach' (Yeh and Tripathi, 1989), or 'global implicit method' (Steefel and MacQuarrie, 1996). Mathematically, the method consists of combining the transport equations so as to eliminate reaction terms. This leads to linear combinations of species (components) that are transported conservatively. Such combinations are unaffected by equilibrium reactions. Since components are conservative, they can be transported easily. Species are then obtained using conventional speciation routines. Equilibrium aqueous speciation and calcite dissolution constants were taken from PHREEQC database (Parkhurst, 1995). For the cases modelled here, four species control

actual dissolution (CO_2, H^+, Ca^{2+} and TDS). The remaining ones are either defined by equilibrium aqueous reactions or play a minor role. Salinity (TDS) determines activity coefficients, which are a non-linear function of the mixing ratio, but is rather independent of calcite content, so that it can be handled separately from the rest. The three remaining species are linked by calcite equilibrium. This means that the number of transport equations can be reduced from three to two by an adequate selection of the components to be transported (Saaltink et al., 1998). Thus, instead the usual set of components, total calcium, inorganic carbon and acidity (or alkalinity), only two components are sufficient to fully describe the system.

For each time increment, the porosity, ϕ_m, is updated according to:

$$\phi_m(t+\Delta t) = \phi_m(t) + r_m V_m \Delta t \qquad (6.2)$$

where V_m is its molar volume ($m^3\,mol^{-1}$), r_m is the rate of mineral precipitation (mol $m^{-3}s^{-1}$), and Δt is the time increment.

6.3. 1D- Diffusive water mixing

6.3.1. Fully coupled reactive transport modeling

Three types of water interact in the mixing zone of coastal aquifers: (1) freshwater that comes from inland, (2) saltwater, which is denser, and flows slowly from the sea, and (3) brackish water, which results from mixing, and flows upwards along the mixing zone. Understanding the interactions of these three waters with transport processes is complex. Therefore, we first simplify the problem by ignoring the brackish component.

The resulting problem is essentially one-dimensional because isohalines are parallel to flow lines and mixing occurs by transverse dispersion. We emulate this problem by considering diffusion across a 1D calcite sample. The problem is scaled down to laboratory conditions. Thus, a 1 cm long sample is considered. 1D-modeling represents a mixing line having prescribed concentrations at the two sides: saline groundwater equilibrated with calcite (solution #3, Table 6.1) on the right-side, and freshwater (solutions #4 through 7, Table 6.1, depending on the simulation) on the left-side. Since neither flow nor head gradients were defined, chemical species were transported by pure diffusion. In each case, the low salinity end-member solution was used as initial condition for the whole geometry, although results are virtually insensitive to initial conditions. The domain was divided in 40 linear elements of equal length and simulations run for 2 years with time steps of 1 day. Parameter values used were: initial porosity, 0.3; and molecular diffusion coefficient (same for all species), 10^{-5} cm^2s^{-1}. Temperature was 25ºC in all the simulations.

Figure 6.1a displays the calcite saturation distribution in a non-reactive medium for a mixture of saline groundwater in equilibrium with calcite ($P_{CO2}=10^{-1.96}$) and freshwater ($P_{CO2}=10^{-2.0}$) (solutions #3 and 4, respectively, Table 6.1). This distribution is compared with the curve of cumulative change in calcite volumetric fraction (expressed as % porosity change), after 100 days of mixing in a carbonate reactive medium (Figure 6.1b). Because of non-linear effects, mixed waters are undersaturated with respect to calcite throughout the domain, with maximum undersaturation towards the freshwater side (mixing ratio around 0.15). However, when a calcite reactive medium is assumed (under local equilibrium), maximum dissolution is obtained at the freshwater end of the column (Figure 6.1b). In other words, dissolution occurs in the mixing zone under much fresher conditions than predicted by non-reactive mixing. The fact that maximum dissolution rate is always found at the second node of the grid, regardless of grid size (recall that concentrations are prescribed to be in equilibrium at the first node) suggests that maximum dissolution occurs at the freshwater boundary. This observation implies that, indeed, the interaction between transport processes and chemical reactions affects dissolution patterns significantly.

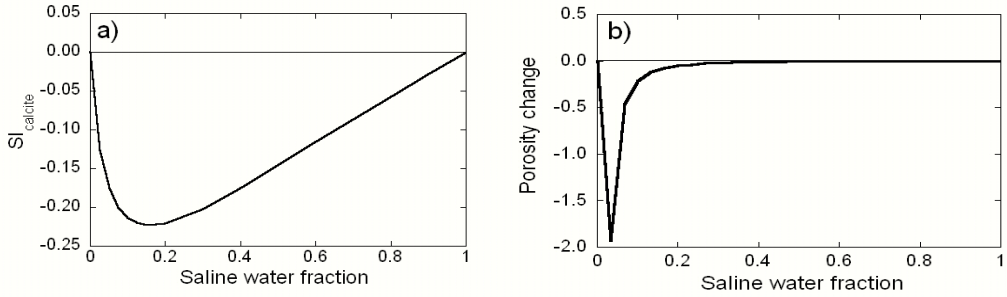

Figure 6.1: Linear mixing of fresh and saline groundwaters equilibrated with calcite (solutions #4 and 3, respectively, Table 6.1): a) Calcite saturation index for a non-reactive mixing; and b) Cumulative change in calcite volumetric fraction (expressed as % porosity change) after 100 days of mixture in a carbonate reactive medium (negative implies dissolution). Calculation done for a 1 cm long domain divided in 40 linear elements of equal length. In each graph freshwater is at the left and saline water at the right.

Figure 6.1 is somewhat paradoxical because one would expect the maximum dissolution of calcite to take place at the location of maximum undersaturation. In order to understand it, let us look in detail at the distribution of the involved aqueous species (Figure 6.2). It is apparent that the concentration of the major species, such as Ca^{2+} is barely affected by dissolution. It increases slightly with respect to the non-reactive case because of calcite dissolution. CO_3^{2-} displays a similar trend, only more marked due to changes in speciation (the increase of pH causes by itself an

increase in CO_3^{2-}.Notice, however, that the actual change is very small (units are μmol/kg_{water} for CO_3^{2-})

On the other hand, dissolution causes a reduction of CO_2(aq) and H^+, thus dramatically increasing the concentration gradient (notice that the vertical scale is logarithmic) and, therefore, the diffusive transport of CO_2(aq) and H^+ at the freshwater side. Since undersaturation conditions are found immediately upon entrance, dissolution occurs immediately, further fostering the process. Dissolution also causes the gradients of CO_2(aq) and H^+ species to be reduced further down towards the saline end-member, thus reducing the dissolution rate progressively.

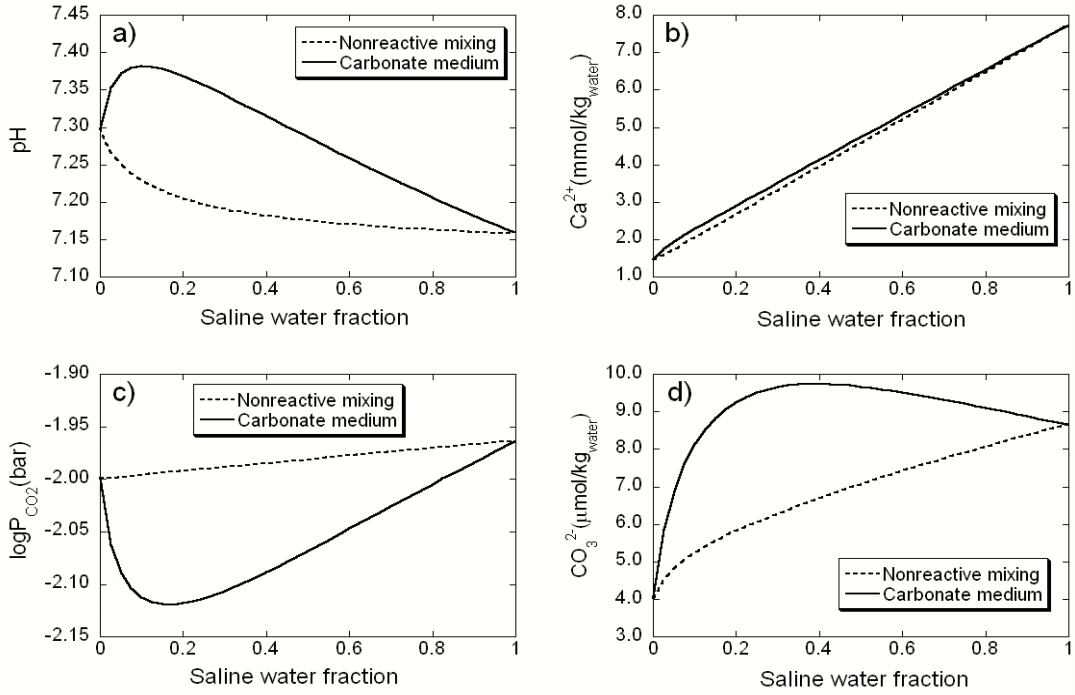

Figure 6.2: Distribution of pH, log P_{CO2}, Ca^{2+} and CO_3^{2-} concentration as a function of the mixing ratio (expressed as saline water fraction), for a non-reactive medium, and for a carbonate reactive medium. End-member solutions are fresh and saline groundwaters equilibrated with calcite (solutions #3 and 4, respectively, Table 6.1). Notice that CO_3^{2-} units are μmol/kg_{water}.

In summary, what causes dissolution to concentrate at the freshwater side of the column is the imbalance between the transport of some species (Ca^{2+} CO_3^{2-}) with respect to the others (CO_2(aq) and H^+).

6.3.2. Two-step method modeling

In order to simulate calcite dissolution in the mixing zone, Sanford and Konikow (1989) used a two-step method consisting basically of (1) transporting TDS and dissolved calcite, (2) evaluating at each node the dissolution potential (derived from the mixing ratio), and (3) dissolving the deficit. The amount of calcite dissolved for each mixture of fresh and saline groundwater) was calculated with the PHREEQC code (Parkhurst, 1995), resulting the curve A in Figure 6.3.

The procedure can be formalized. First, solving the transport equation for dissolved calcite (TDS is computed from the mixing ratio) as:

$$\frac{c^{k+1} - c^{k}}{\Delta t} \cong \frac{\partial c}{\partial t} = D\frac{\partial^2 c}{\partial x^2} \qquad (6.3)$$

where k is time step number. This causes the equilibrium curve A to get displaced towards curve B. Second, dissolution is simulated by bringing c^{k+1} back to the equilibrium concentration c_{eq} (curve A in Figure 6.3). Third, dissolution rate is computed as:

$$r = \frac{c_{eq} - c^{k+1}}{\Delta t} \qquad (6.4)$$

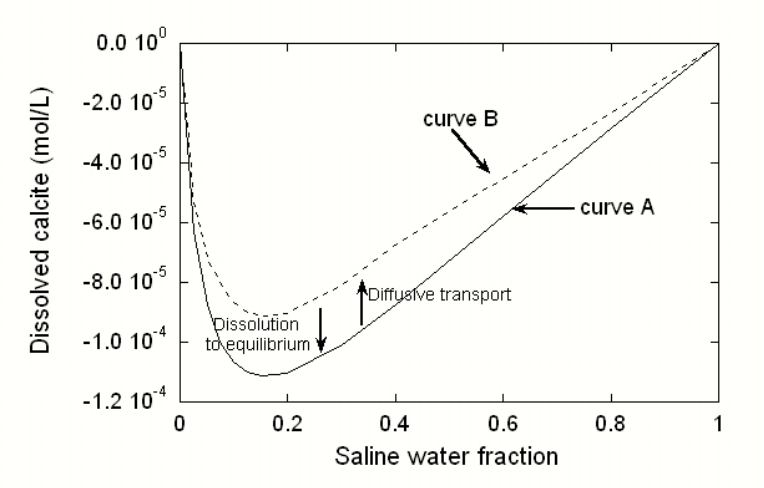

Figure 6.3: Schematic description of the two-step method. Curve A indicates the amount of calcite dissolved to reach equilibrium for each mixing ratio. Diffusion during one time increment (step 1) smoothes this curve up to curve B. The difference must then be dissolved (step 2) to ensure equilibrium.

Three points should be noticed. First, all time steps are identical (initial concentrations for each time step are given by curve A). Second, dissolution rate is proportional to D, that is to mixing rate. Third, the procedure works for small time steps, because concentration change ($c^{k+1} - c^{k}$ in eq 6.3)

is proportional to Δt. However, as Δt grows, the rate of change is reduced, so that for large Δt, the rate tends to decrease. It should be noted that a similar effect occurs for space discretization. That is, the maximum dissolution rate increases when increasing Δx.

To evaluate the importance of this effect, we performed the calculations for several time steps and compared them with a fully coupled simulation. Results are shown in Figure 6.4.

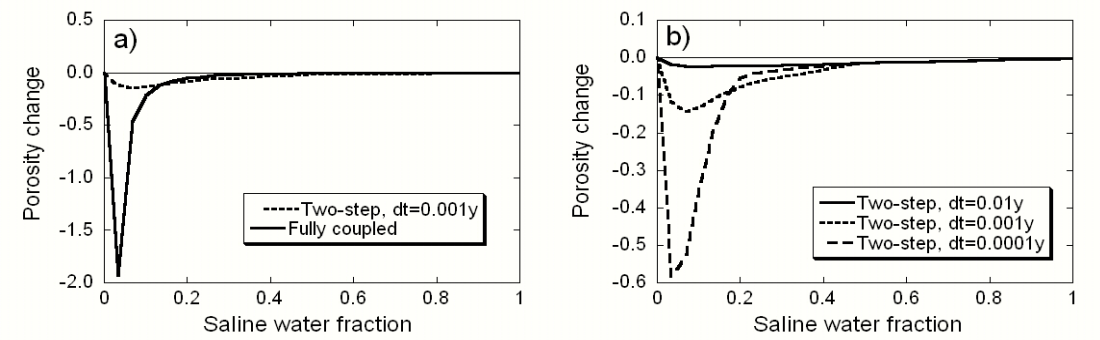

Figure 6.4: Performance of the two-step method for mixing solutions #3 and 4 (Table 6.1) across a calcite sample: a) comparison with fully coupled reactive transport for a time increment of 10^{-3} y; b) results of the two-step method for time increments of 10^{-2}, 10^{-3} and 10^{-4} y.

The amount of calcite dissolved with the two-step method is too small and, the maximum dissolution takes place further away from the freshwater end of the sample (Figure 6.4a). Moreover, as the time step is reduced calcite dissolution increases and the maximum dissolution location is shifted towards the freshwater end-member (Figure 6.4b). Results of the fully coupled method, however, are independent of the time increment.

The dependence of both dissolution rate and total calcite dissolved with respect to time increment is shown in Figure 6.5. Results are accurate for the grid characteristic diffusion time ($\Delta t < 0.1\Delta x^2 / D = 2.10^{-6}\,y$). Otherwise, dissolved calcite is underestimated. In fact, for $\Delta t > L^2 / D = 2 \cdot 10^{-3}\,y$, characteristic time for equilibrium across the sample, diffusion would tend to bring curve A (Figure 6.3) to the horizontal axis. That is, dissolution during a time step would reach its maximum, thus becoming independent of the time step duration. This implies that reaction rate would become inversely proportional to Δt.

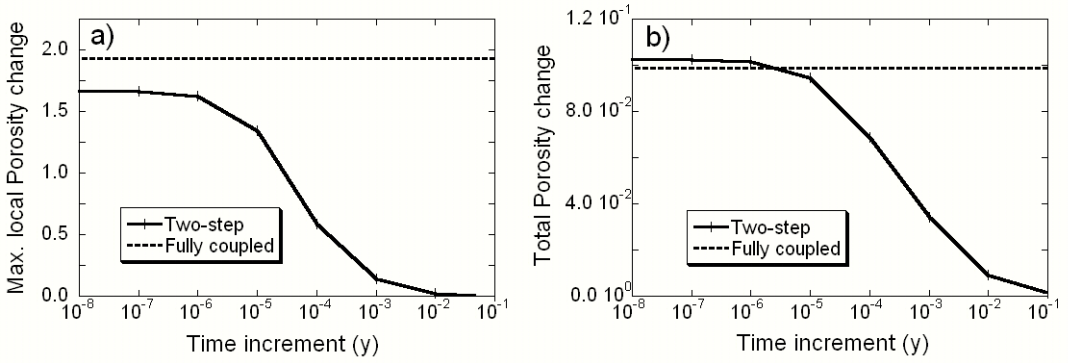

Figure 6.5: Time increment dependence of a) maximum, and b) total (spatially integrated) change in calcite volumetric fraction (expressed as % porosity change) using the two-step and the fully coupled approaches. Notice that dissolution rate computed with the fully coupled method is independent of the time increment.

6.3.3. Dependence of the dissolution on the chemistry of end-members

As discussed in the introduction, dissolution processes in the mixing zone are known to depend on a large number of factors (mainly the differences in species total concentration, pCO_2, pH and ionic strength of end-members). Therefore, the porosity development will be sensitive to the pCO_2 of the end-members as well as the chemistry of the entire system.

Results up to here indicate that one critical parameter is P_{CO2}. When maintaining the saturation with respect to calcite, a decrease of P_{CO2} is linked to increase in pH (solutions #4 and 5, Table 6.1). As pointed out by Sanford and Konikow (1989), a decrease in P_{CO2} in the freshwater end-member solution leads to a reduction of calcite undersaturation and, accordingly, a slower dissolution rate. Figure 6.6a shows such effect, (solutions #3 and 4, or 5, Table 6.1). Surprisingly, calcite dissolution displays the opposite behaviour. That is, dissolution rates decrease with the increase of P_{CO2} of freshwater end-member (Figure 6.6c). In short, the behaviour of the saturation index is contrary to that of dissolution rate. This can also be attributed to the interplay between transport and reactions. As shown by Figure 6.2, dissolution enhances transport of H^+ and $CO_2(aq)$, and thus further dissolution. However, in the case of Figure 6.6, this effect is relatively minor when the P_{CO2} of freshwater is $10^{-3.0}$ bar, because the freshwater boundary concentrations of CO_2 and H^+ are small. This causes the diffusive transport of acidity and, hence, dissolution rate to be small. On the other hand, the transport of acidity is relevant when the P_{CO2} of freshwater is $10^{-2.0}$ bar. It is worth noting that the opposite occurs in the saline water half of the mixing, where dissolution rate decreases with the P_{CO2} of freshwater (Figure 6.6e). Here, transport distances are much larger and dissolution of calcite much smaller, so that the depletion in P_{CO2} caused by dissolution does not cause a significant increase in H^+ and $CO_2(aq)$ transport. Under these conditions, the dissolution

rate is controlled by the saturation index effect (Figure 6.6a) and dissolution rate is larger for large contrast of P_{CO2} in fresh and saltwater, as usually stated (Wigley and Plummer, 1976).

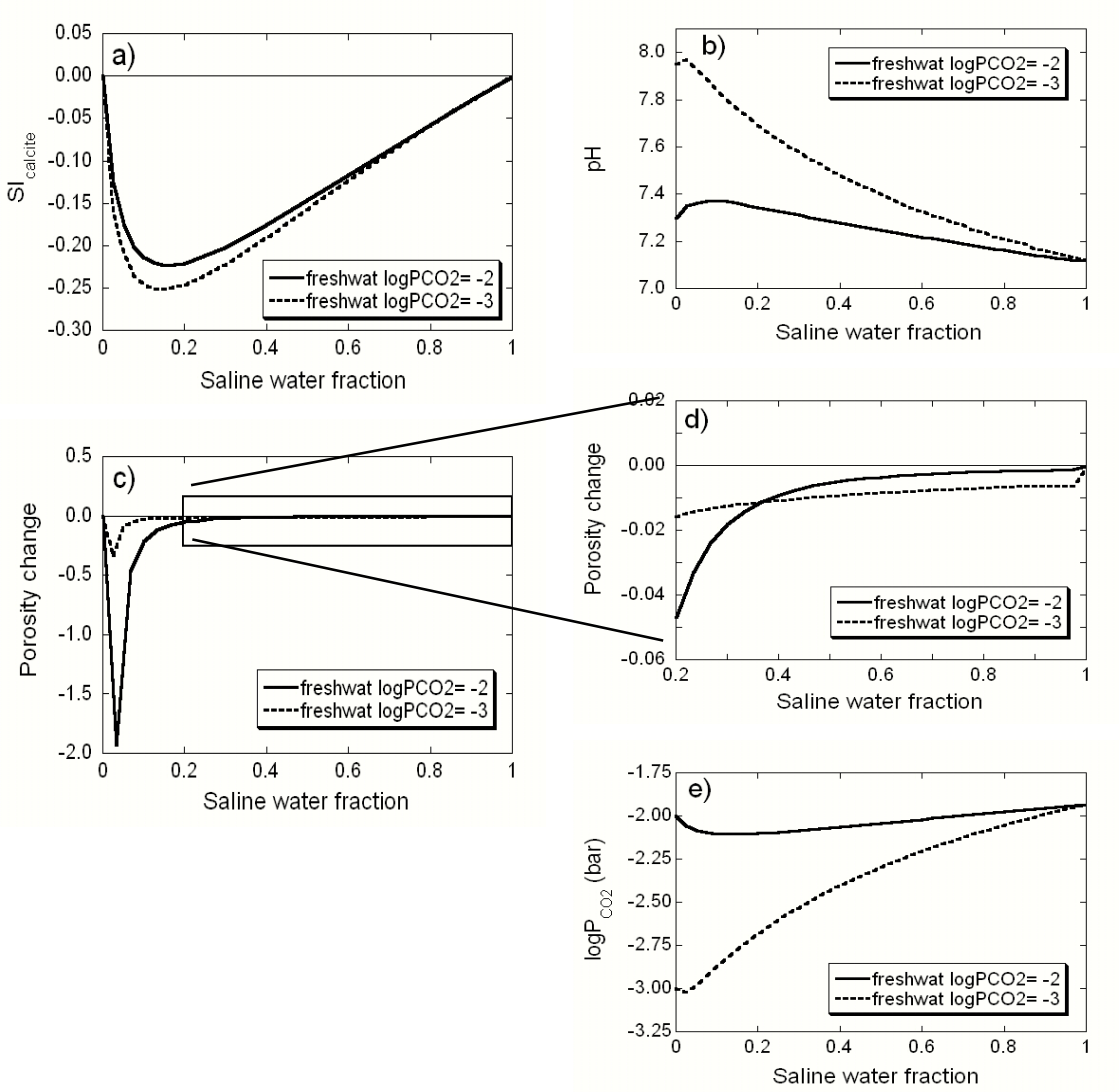

Figure 6.6: Sensitivity of mixing to the P_{CO2} of end-members (solutions #4 and 5 for freshwater and 3 for saline water, Table 6.1) a) Calcite saturation index; b) pH; c) porosity change after 100 days of mixture in a carbonate reactive medium; d) blow up of figure c); and e) log P_{CO2} distribution.

Changes in the chemistry of the saline end member will also change the amount of dissolved calcite. We compared simulations using different saline end-member solutions: saline groundwater (as we did up to here) or open ocean water (Sanford and Konikow, 1989) (solutions #2 and 1, respectively, Table 6.1). Mixture with open ocean water was slightly less undersaturated than that with saline groundwater, but the results (not shown) were not affected qualitatively.

As was explained before, the calcium concentration is strongly dependent on the geochemical evolution of the solution through the aquifer soil. We consider the mixing of a saline groundwater

equilibrated with calcite (Solution #3, Table 6.1) with freshwater equilibrated with calcite and $P_{CO2}=10^{-2.0}$, but different calcium and H^+ concentrations (Solutions #4, 6 and 7, Table 6.1).

Figure 6.7 compares the results obtained for a non-reactive and reactive mixing in each case. The calcite undersaturation in a non-reactive medium is reduced for pH 6.97 and leads to oversaturation for pH 7.73 (Figure 6.7a). These trends are reproduced in terms of calcite dissolution in a reactive carbonate medium (Figure 6.7b). The oversaturation for pH 7.73 is the result of high divergence on calcium concentration of the two end-members. Since calcium does not speciate with pH, these differences enhance the algebraic effect. On the other hand, for pH 6.97 the algebraic effect is small compared the ionic strength effect. In other words, the solution with pH 6.97 presents an ionic strength one order of magnitude higher than the other freshwater solutions, reducing the ionic strength difference with respect to the saline end-member. The result leads to slight calcite dissolution.

The most important conclusion from this 1D analysis is that one needs to couple chemistry and transport to understand dissolution dynamics. Chemistry (i.e. end members concentrations) controls dissolution potential. Transport processes (mixing) control how much, when, and where dissolution occurs. First, and foremost, dissolution rate is proportional to mixing rate (D in our case). Second, the interplay of transport and chemistry leads to non-trivial conclusions or a-priori guesses. In this 1D example, enhanced CO_2 transport at the freshwater end causes dissolution rate to be maximum there (far from where non-reactive mixing would have led to maximum undersaturation). Moreover, transport may also cause an increase in dissolution rate contrary to what saturation indeces would have suggested (recall Figure 6.6).

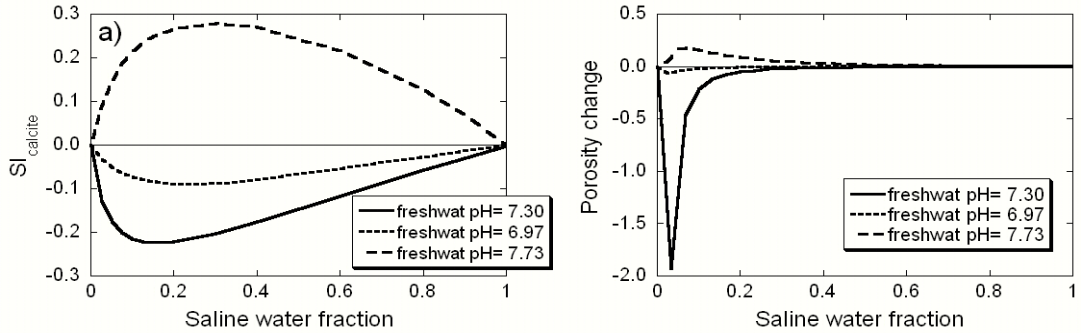

Figure 6.7: Diffusive mixing of saline groundwater (solution #3, Table 6.1) and freshwater equilibrated with calcite at different pH values (solution #4, 6 or 7, Table 6.1). a) Calcite saturation index distribution in a non-reactive medium; b) cumulative change in calcite volumetric fraction (expressed as % porosity change) after 100 days of mixture in a carbonate reactive medium. Porosity change is positive for precipitation and negative for dissolution.

6.4. 2D-Flow and reactive transport modeling

A two-dimensional cross-section, perpendicular to the shore, was simulated to quantify porosity development in a carbonate aquifer. The problem set-up is similar to that of Sanford and Konikow (1989). Simulating carbonate dissolution in a coastal aquifer requires defining not only hydrogeochemistry of the system but also the layout of fresh and saltwater, which is a density dependent flow problem. The governing equations are a set of two partial differential equations representing groundwater flow and salinity transport (see Bear, 1972; Voss and Souza, 1987, for details). These equations are non-linearly coupled because the flow equation depends on density, which is a function of salinity, and the transport equation depends on the flux. We solved them by means of the finite element program CODE-BRIGHT (Olivella et al, 1994), which uses a Newton-Raphson scheme for dealing with non-linearities and coupling.

The domain is a 100 m deep and 1500 m long calcite rectangle, discretized into a finite element grid consisting of 9459 triangular elements and 4954 nodes. The grid is somewhat refined in the mixing zone, where element sizes are about 5 m (Figure 6.8). The shore line is located 250 m to the left of the upper right corner. A column of constant hydrostatic seawater head is prescribed at the right boundary. Constant seawater level is also assumed for the rightmost 250 m of the top boundary, where shallow ocean water is represented by means of a zero prescribed pressure. A flux condition is prescribed for transport across these boundaries, with the salinity flux equal to water flux times seawater salinity for the inflowing portions, or resident salinity for the out flowing portions. Freshwater inflow is specified at the left boundary to represent input from an inland aquifer (constant flux of 250 m y^{-1}) and at the left 1250 m of the top boundary, to represent a constant surface recharge of 0.5 m y^{-1}. The bottom of the system is a no-flow boundary. Permeability is constant and equal to 7.4×10^{-10} m^2. Longitudinal and transverse dispersivities are set to 6 and 3 m, respectively, and initial porosity to 0.3.

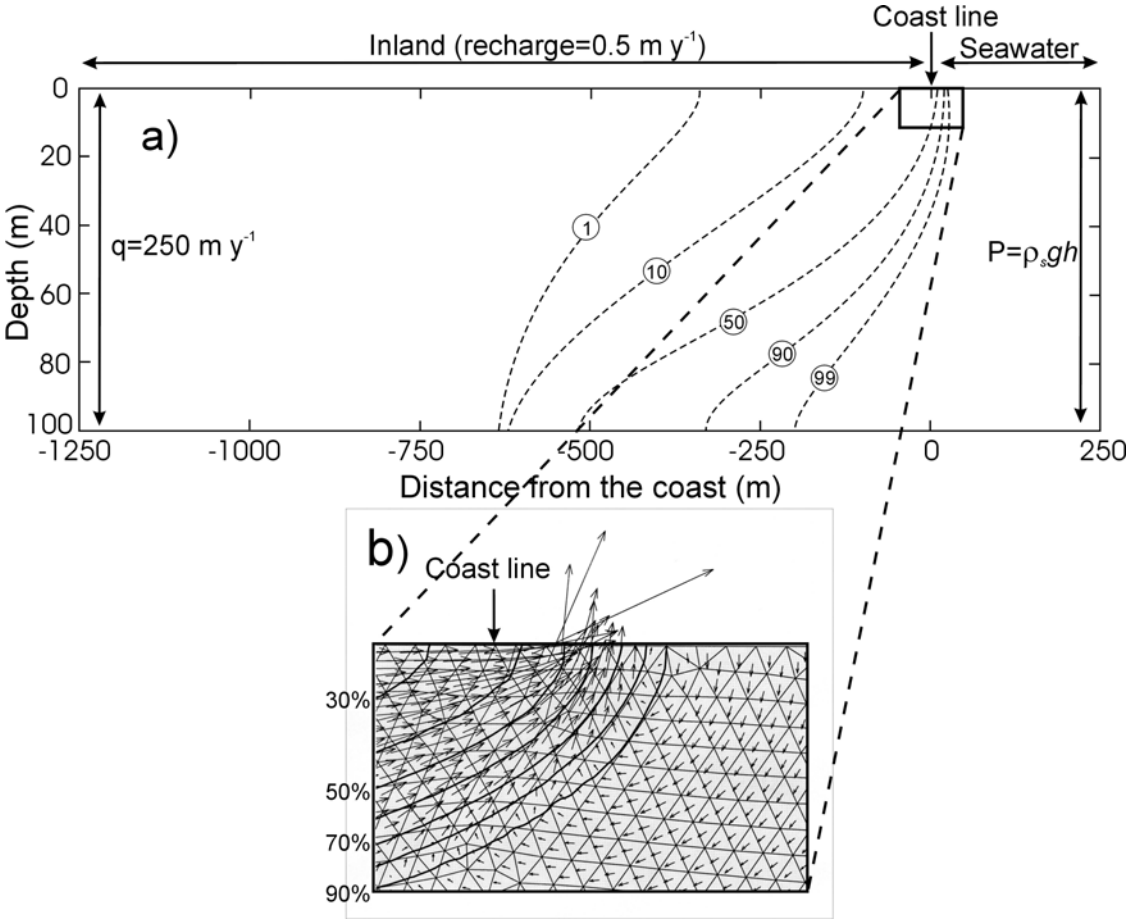

Figure 6.8: a) Problem set-up of the 2D-cross sectional model, including boundary conditions (where *P* represents Pressure, ρ_s the density of seawater, *g* the gravity, *h* the depth with respect to sea level and *q* the freshwater flow source in the left boundary). The curves display the position of 1, 10, 50, 90 and 99% seawater mixing ratios (left to right); b) Blow-up showing the grid, the flow field and the position of 30 to 90% (every 10%) of seawater, for the area near the discharge area. Arrow lengths are not exactly proportional to velocity values, for figure simplification, and are shown to represent the flow direction in every element. Vertical scale is exaggerated 5 times in Figure 6.8a).

The resulting steady-state mixing zone displays the expected shape with freshwater discharging along the coastline, while floating on top of higher salinity water (Figure 6.8). The most significant feature of this model is the convective cell near the shore, which explains the high salinity gradient at the seaside top of the mixing zone. The presence of this cell is relevant because it enhances mixing of fresh and seawater near the exit point, and a chemically reactive mixture near this area is likely to occur. However, its shape and size in reality is somewhat uncertain. The model solution near the shore is unstable because seawater overlays the less dense outflowing water. As a result, fingering is likely to occur, which we do not simulate because we assume a steady state flow

regime. Despite these instabilities, our problem definition was rather robust since consistent results were obtained irrespective of grid size and dispersivity values.

Inland freshwater flows seawards on top of saline groundwater until it discharges at the coast (Figure 6.8). Depending on coastal topography, discharge may take place above (as discussed here) or below sea level. Seawater, on the other hand, flows inland, until it reaches freshwater and both solutions mix. Freshwater finally carries mixed seawater upwards back to the coast. This mixing drives the flux of groundwater, which is very small at depth, and become sub parallel to the equal salinity lines in the mixing zone. As a result, concentrations are there basically controlled by advection and longitudinal dispersion from downstream (where dissolution may have taken place) and lateral dispersion from the fresh- and seawater sides. This transport complexity, added to the strong sensitivity of the dissolution to the geochemistry of the system (see discussion above) makes it necessary to extend the study to a 2D-fully coupled reactive transport model, in order to better describe calcite dissolution and porosity development in the mixing zone. These simulations were performed by coupling CODE-BRIGHT and RETRASO codes.

As reference case, we used as end-members freshwater equilibrated with calcite under $P_{CO2}=10^{-2.0}$ (solution #4, Table 6.1), and saline groundwater from Grand Cayman coastal aquifer (solution #2, Ng and Jones, 1995, Table 6.1). Porosity change, after 10,000 years of calcite dissolution, is shown in Figure 6.9. Dissolution takes place along the whole mixing zone, although two locations concentrate the maximum dissolution: one at the toe (aquifer bottom) and another, more important, at the coastal discharge area. This distribution is qualitatively similar to the one obtained by Sanford and Konikow (1989). This shows that, despite the difficulties discussed previously, their method captures the essence of the problem.

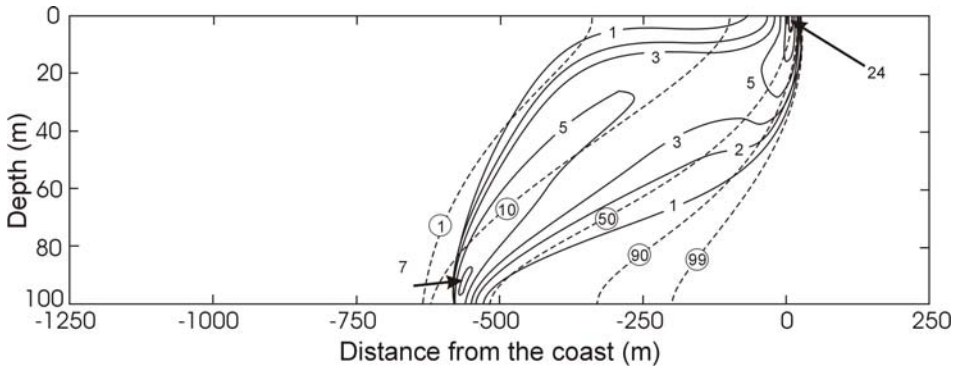

Figure 6.9: 2D-porosity development computed with a fully coupled reactive transport code after 10^4 years. End-member solutions are freshwater equilibrated with calcite under P_{CO2} of $10^{-2.0}$, and saline groundwater (solutions #4 and 2, respectively, Table 6.1). Results are expressed as rates of porosity change every 10,000 years, in %). Vertical scale is exaggerated 5 times.

The dissolution maximum at the toe is caused by the fact that only fresh and seawaters are mixing (i.e. there is no mixing zone contributing from below). The controlling factor is the seawater flux, which is very small there. In fact, the flux should be zero at the very bottom, which explains why the maximum is slightly displaced above the bottom boundary. It is clear that proper evaluation of dissolution rate requires a rather fine grid for accurate computation of seawater fluxes. Along the mixing zone, maximum dissolution rates generally occur towards the freshwater side, except near the exit.

The absolute, maximum dissolution takes place close to the discharge area, with a maximum porosity increase rate of 24% every 10,000 years. This porosity development is consistent with the formation of Pleistocene cavities in the Bahamas, which took place (according to the sea level changes) during a period of time shorter than 25,000 years (Mylroie and Carew, 1990). It is interesting to notice that the maximum dissolution is located towards the saltier side of the mixing zone, which is apparently inconsistent with the results obtained for pure diffusive mixing (see discussion above), where the maximum dissolution rates were always was found near the freshwater side. We attribute this apparent paradox to the fact that, in our case, dispersive mixing at the upper part of the aquifer, close to the coast, is much more active at the saline side than at the freshwater side (notice that the convection cell shown in Figure 6.8b, causes the isolines to be much closer in the saline than in the freshwater side). That is, this dissolution spot is related to the presence of the active convection cell near the coast. This enhances mixing and dissolution. Modeling of this circulation cell requires a fine discretization. Since the situation is unstable (dense water on top), a transient simulation would be needed. Moreover, actual details of mixing processes there will be sensitive to local conditions (heterogeneity, tides and the like).What is clear is that computed porosity development is likely to be a significant underestimation. In addition, the increase in porosity should yield an increase in permeability, thus further fostering seawater flow and dispersion, which may become turbulent.

1D-diffusive mixing simulations showed that the effect of P_{CO2} on dissolution potential is very large, with the two end-members significantly affecting dissolution. Consequently, we analyse here the effect of P_{CO2} on porosity development. The rate of porosity change is shown in Figure 6.10 for simulations considering combinations of both high and low P_{CO2} in both end-members (involving solutions #1, 2, 4 and 5, Table 6.1). Results appear to be consistent, both in terms of inflowing freshwater P_{CO2} and porosity development.

In general, differences in P_{CO2} between the end-member solutions results in an increase of total accumulated calcite dissolution. Still, a number of results deserve further discussion. First of all, for a similar P_{CO2} value in both end-members, dissolution rate increases with P_{CO2} (Figure 6.10b and c). As discussed above, CO_2 (i.e., alkalinity) generated by dissolution is depleted faster for high

P_{CO2} and dissolution rates are lager (Figure 6.10b). Still, maximum porosity development is produced for the case mixing high P_{CO2} freshwater and low P_{CO2} saline water because the two effects (large differences between end members and high P_{CO2} of freshwater) sum up (Figure 6.10a).

On the other hand, the situation is a bit more complex for the opposite case, i.e. when the P_{CO2} for saline water high and low for freshwater (recall that it was also more complex in pure mixing, Figure 6.6). These results should be compared with the reference case (Figure 6.10b). The maximum dissolution rate near the toe disappears when the P_{CO2} of freshwater is low (Figure 6.10d). This is consistent with the important reduction of the dissolution rate displayed near the freshwater side under these conditions in Figure 6.6, which was attributed to the relatively low transport of H^+ and CO_2(aq) from freshwater. Under those conditions, it was also showed that, near the saline side, dissolution was enhanced relative to that of high P_{CO2} freshwater. That situation was attributed to the enhanced undersaturation (and hence dissolution capacity) of simple mixing, and explains why the dissolution maximum at the discharge zone is now very large (Figure 6.10a).

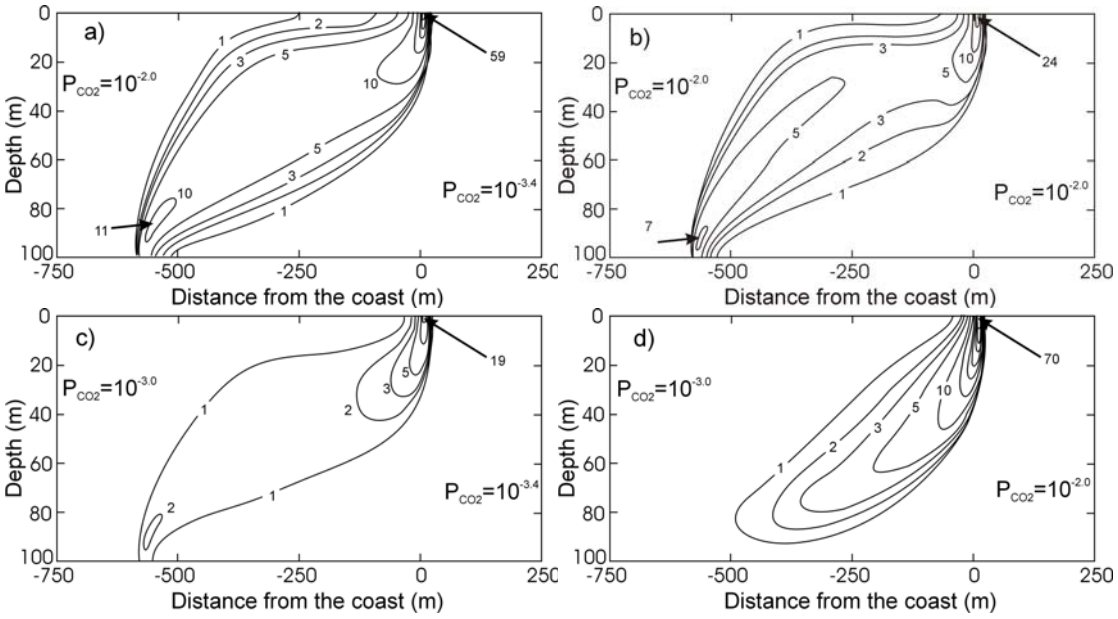

Figure 6.10: 2D-porosity development after 10,000 years, showing the effect of the P_{CO2} of the two end member solutions. Simulations mixed freshwater under P_{CO2} of $10^{-2.0}$ or $10^{-3.0}$, and either open ocean or saline groundwater (solutions #4, 5, 1 and 2, respectively, Table 6.1). Results are expressed as rates of porosity change every 10,000 years, in %). Vertical scale is exaggerated 5 times.

The fact that dissolution rates at the discharge area increase with the difference in P_{CO2} of fresh and saline waters is well known to occur in tropical areas, like Yucatan or Bahamas. There, the P_{CO2} of freshwater is expected to be high (from $10^{-2.0}$ to $10^{-1.5}$ bar according to Brook et al., 1983)

and low P_{CO2} saline water may occur when organic matter degradation is low. However, the low P_{CO2} of freshwater in arid areas, such as the Mediterranean coasts of Spain or Italy, is usually taken as an indication of low dissolution capacity or even oversaturation (Price and Herman, 1991). Our results suggest that, when the P_{CO2} of the saline end member is high, the opposite will occur. That may explain dissolution processes at the Garraf near Barcelona (Pascual and Custodio, 1987), where saline groundwater near the coast shows P_{CO2} values as high as $10^{-1.5}$ bar, due to the high organic matter concentration from Barcelona sewage discharges. Well developed cave formations are found at the fresh-salt water boundary.

Discussions up to here imply that dispersivity is a very important parameter, and unfortunately, there is no clear criterion for assigning it in seawater intrusion problems. Empirical large scale values often fall around one tenth of the size of contaminant plumes. The mixing zone dimensions in our case are 100 m in the vertical direction and around 500 m in the horizontal, suggesting longitudinal dispersivity between 10 and 50 m. However, these values are only valid for a time evolving plume and would not be appropriate for reactive transport, because they yield the overall size of the plumes, but do not represent local mixing appropriately. Smaller dispersivities should be used for essentially steady state transport. In fact, Abarca et al. (2005) show that effective dispersion for seawater intrusion in heterogeneous media is close to the local value of dispersion. Time fluctuations in the velocity field, usually caused by seasonal variations of recharge, may be important in most coastal aquifers, where the effect of tides is added. The net effect of these fluctuations in a heterogeneous medium is a sizeable increase in dispersivity (Dentz and Carrera, 2003). We have chosen a minimum value of 6 m for longitudinal and 3 m for transversal dispersivity for numerical reasons, but the value of 1 m adopted by Sanford and Konikow (1989), could be valid as well. It is therefore clear that the effect of uncertainty in dispersivity must be analyzed.

The effect of dispersivity is analyzed by comparing the results obtained for simulations that combined longitudinal dispersivities of 6 or 15 m with transversal dispersivities of 3 or 6 m. End-member solutions are those of the reference case (solutions #2 and 4, Table 6.1). Results are shown in Figure 6.11.

The toe position provides a preliminary check on results. Increasing dispersion (especially transverse dispersion) causes an increase in seawater flux, so that the toe is displaced seawards, which can indeed be observed in Figure 6.11. Indeed, the zone of maximum dissolution at the bottom of the aquifer shifts from around 600 m for longitudinal and transversal dispersivities of 6 and 3 m, respectively (Figure 6.11c), to around 450 m for dispersivities of 15 and 6 m (Figure 6.11a).

Overall dissolution tends to increase with dispersivity, as expected, because it causes an increase in mixing rate. This is especially true at the bottom dissolution spot. The middle portion of

the mixing zone remains unsensitive to the longitudinal dispersivity (Figure 6.11b and c) because mixing in this portion is mainly controlled by transverse dispersion. On the other hand, increasing transverse dispersivity (Figure 6.11a and b) leads to an increase in the width of this portion, but not in maximum dissolution. Moreover, the maximum dissolution near the discharge area is significantly decreased for higher longitudinal dispersivity values. We attribute this reduction to the increase in the flux of mixed water, which has reduced significantly its dissolution potential and which is reaching the discharge area from underneath (recall the convection cell inset in Figure 6.8b).

To conclude, the dependence of dissolution on dispersivity is non-monotonic. Increasing transverse dispersion does not necessarily cause a parallel increase in dissolution at the maxima. Still, significant dissolution occurs for all reasonable values of this parameter, so that the conclusions can be considered robust.

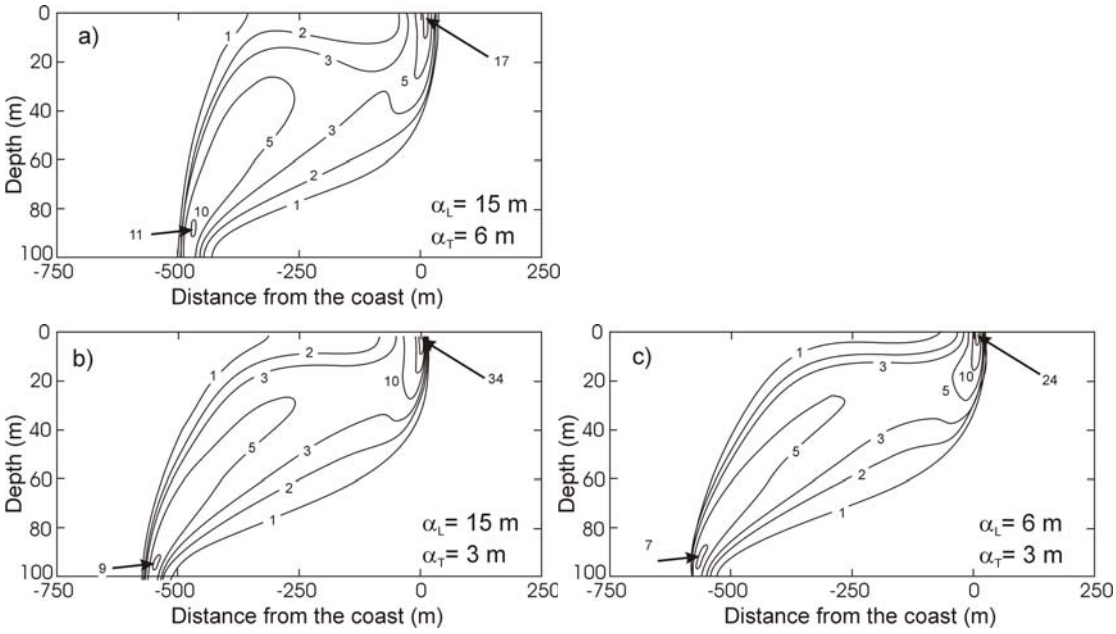

Figure 6.11: 2D-porosity development after 10,000 years, showing the effect of longitudinal and transverse dispersivity. Dispersivity values were 15 or 6 m, for longitudinal, and 6 or 3 m , for transverse. End-member solutions for all cases where those of the reference case (solutions #2 and 4, Table 6.1). Results are expressed as rates of porosity change every 10,000 years, in %). Vertical scale is exaggerated 5 times.

6.5. Conclusions

Results presented here provide insight on the interplay between chemistry and transport in the mixing zone of coastal carbonate aquifers. Simulations performed of one dimensional mixing (diffusion) show that it is the transport of minor acidity constituents (CO_2(aq) and H^+) what largely

controls the system. They are depleted by calcite dissolution, which increases their diffusion rate, further increasing dissolution. This causes maximum dissolution rates to concentrate at the freshwater end. As expected, the amount of calcite dissolved is larger for the fully coupled than that for the two-step method, which only converges for time steps sufficiently small.

The interaction between reactions and transport also explains the somewhat paradoxical dependence of dissolution rates on the P_{CO2} of end members. The most interesting situation occurs when the P_{CO2} of saltwater is high. This has been observed in saline groundwaters and attributed to organic matter degradation processes. Under these conditions, undersaturation increases with decreasing P_{CO2} of the freshwater end member. However, the opposite occurs to dissolution rates near the freshwater end member, because the transport of acidity can be larger for high freshwater P_{CO2}. On the other hand, near the saline end member, diffusion distances are long, so that the effect of saturation index prevails and dissolution is largest for low freshwater P_{CO2}.

The above results suggest that indeed the interplay between transport and reactions is non-trivial. Saturation index calculations are needed but do not indicate how much calcite is dissolved, which is controlled by mixing rate, nor necessarily where dissolution rate is maximum. This supports our conjecture about the need for fully coupled reactive transport. Therefore, we proceeded to perform simulations of mixing zone dissolution processes in a 2-D vertical cross-section of a hypothetical coastal carbonate aquifer. Our results are qualitatively similar to those obtained by Sanford and Konikow (1989), despite the fact that they only transported one component (dissolved calcite), as opposed to the minimum of two we argue is necessary. This implies that their approach works better than we had anticipated. Still, our results allow one to gain some additional insights into the process.

As obtained by Sanford and Konikow (1989), two locations of maximum dissolution rates are found: one near the aquifer bottom and one near the discharge area, with some residual dissolution occurring throughout the rest of the mixing zone. In general, dissolution tends to concentrate at the freshwater side of the mixing zone, except at the discharge area, where dissolution is maximum near the saline side. This contrasts with Sanford and Konikow's results, but agrees with calcite subsaturation observed in some blue holes from Bahamas (Whitaker and Smart, 1997). Dissolution rates in this area are consistently larger than elsewhere and can be very high. Results are relatively robust with respect to dispersivity, which is fortunate because of the uncertainties in assigning this parameter.

The largest dissolution rate at the discharge area is caused by the very active convection cell that develops there. In fact, positive feedback processes that have not been simulated here can further enhance dissolution at the discharge area. Dissolution will cause an increase in permeability. This would enhance further seawater flow and mixing in the simulated cross-section.

Moreover, heterogeneities would cause dissolution to be uneven along the coast. This would lead to three-dimensional effects, causing flow from adjacent flow lines to concentrate in the locations of initial dissolution. The result would be dissolution rates even higher than those predicted here.

Calcite dissolution rate at the discharge area is larger when the P_{CO2} of both end members are very different. This is consistent with the saturation indices computed from non-reactive mixing, but unexpected in view of the dissolution rates obtained with 1D-reactive transport simulations. We attribute it to the fact that dissolution at the discharge area takes place in the saltwater side of the mixing zone, where saturation index effects prevail. This implies that highest rates will occur in tropical areas where freshwater recharge contains high P_{CO2}, but they will be found also in arid regions where freshwater P_{CO2} is expected to be low, provided that saline groundwater contains high P_{CO2} values.